Nature Communications

https://doi.org/10.1038/s41467-025-67882-3

Article in Press

Harnessing multivalency and FcγRIIB engagement to augment anti-CD27 immunotherapy

Received: 10 December 2024

Accepted: 11 December 2025

Cite this article as: Widdess, M.A., Pakidi, A., Metcalfe, H.J. *et al.* Harnessing multivalency and FcγRIIB engagement to augment anti-CD27 immunotherapy. *Nat Commun* (2025). https://doi.org/10.1038/s41467-025-67882-3

Marcus A. Widdess, Anastasia Pakidi, Hannah J. Metcalfe, H. T. Claude Chan, Tatyana Inzhelevskaya, Chris A. Penfold, C. Ian Mockridge, Steven G. Booth, Sonya James, Sean H. Lim, Stephen A. Beers, Mark S. Cragg & Aymen Al-Shamkhani

Harnessing Multivalency and FcγRIIB Engagement to Augment Anti-CD27 Immunotherapy

Marcus A. Widdess[1], Anastasia Pakidi[1], Hannah J. Metcalfe[1], H.T. Claude Chan[1], Tatyana Inzhelevskaya[1], Chris A Penfold[1], C. Ian Mockridge[1], Steven G. Booth[1], Sonya James[1], Sean H. Lim[1], Stephen A. Beers[1], Mark S. Cragg[1] and Aymen Al-Shamkhani[1*]

[1]Antibody and Vaccine Group, Centre for Cancer Immunology, School of Cancer Sciences, Faculty of Medicine, University of Southampton, UK

*Corresponding author, aymen@soton.ac.uk

Abstract

Despite significant clinical progress, checkpoint blockade remains limited by variable response rates, resistance, and toxicity. Activating costimulatory receptors offers a promising alternative to enhance anti-tumor immunity. However, there is insufficient understanding of how to mimic physiological membrane-anchored costimulatory ligands. Here, we describe a strategy for developing effective agonists of the costimulatory receptor CD27 by increasing both antibody valency and FcγRIIB engagement. Engineered anti-CD27 antibodies capable of tetravalent binding to CD27 and selective FcγRIIB association exhibit potent T cell stimulatory activity and anti-tumor efficacy in pre-clinical models, compared to bivalent counterparts. The anti-tumor effects of the tetravalent antibody are mediated through $CD8^+$ T cell activation without evidence of regulatory T cell depletion. Mechanistically, whereas the increase in avidity drives more efficient CD27 clustering, FcγRIIB engagement triggers polarization of receptor clusters to the cell-cell interface and reduces receptor internalization. This work provides a framework for developing more effective agonist-based T cell stimulatory therapies.

Introduction

T cells express unique, somatically rearranged T cell receptors (TCRs) that exhibit a degree of cross-reactivity, thus enabling the recognition of diverse pathogen and tumor derived antigens. To maintain immunological homeostasis, additional receptor-ligand interactions regulate T cell activation through costimulatory or inhibitory signals [1, 2]. It has now been established that immune evasion is a key mechanism by which tumors grow and metastasize [3]. Immune suppression within the tumor microenvironment skews the balance of inhibitory and co-stimulatory signals towards inhibition, leading to T cell ignorance, anergy and exhaustion [4]. Antibody-mediated blockade of inhibitory immune

checkpoints has shown clinical efficacy across multiple cancer types, with CTLA-4 and PD-1 inhibitors demonstrating particular success [5]. However, challenges persist, including variable response rates, development of resistance, and immune-related adverse events [5]. An alternative approach to enhance anti-tumor immunity involves the direct activation of costimulatory receptors. The premise underpinning this strategy stems from the original work demonstrating that activation of CD28 through ectopic B7 expression on tumor cells leads to their elimination by the immune system [4, 6]. Similar findings with other costimulatory ligands and agonist antibodies targeting TNF receptor superfamily (TNFRSF) members have supported the development of clinical agents [4, 7]. However, the majority of clinical agonists have demonstrated insufficient therapeutic activity, the precise reasons for which remain poorly understood [7]. Multiple factors have been shown to influence the activity of agonist anti-TNFRSF antibodies, including epitope, isotype and affinity [8-10]. Receptor clustering by antibodies is generally required for activation of downstream signalling events, a process that mimics the natural interaction of TNFRSF proteins with their trimeric ligands. Thus, murine IgG1 antibodies targeting members of the TNFRSF exert strong agonism dependent on binding to the inhibitory Fcγ receptor (FcγRII) and introduction of mutations into human IgG1 Fc that enhance affinity towards human FcγRIIB similarly bolster agonism [8, 11-13]. Moreover, various antibody engineering approaches have been proposed that enhance TNFRSF agonism by increasing antibody avidity [14-16], or conformational stability [17, 18].

Antibodies that target the T cell costimulatory receptor CD27 have shown promise in enhancing anti-tumor immunity in preclinical models [19-22]. The efficacy and mechanism of action have been shown to be influenced by antibody isotype. For example, the activity of an agonistic anti-CD27 antibody, MK-5890, in both primary human tumor cultures and human CD27 knock in mice, was significantly diminished when the isotype was switched from human IgG1 to IgG2 or a variant that further reduces the interaction with FcγR [23]. However, targeting CD27 with human IgG1, an isotype associated with strong effector function, resulted in depletion of T cells, especially regulatory T cells, calling into question the choice of using the human IgG1 backbone in CD27 agonists [23-25]. Given these uncertainties and the limited clinical efficacy of Varlilumab, a human IgG1 anti-CD27 antibody [25, 26], we sought strategies to generate more effective antibodies with enhanced therapeutic potential.

Here we explore approaches to optimize the agonistic activity of CD27-targeted antibodies and investigate how valency and FcγR engagement shape their activity in both mouse and human systems. Our data show that these mechanisms act synergistically to enhance agonism and anti-tumor efficacy.

Together, these findings outline a strategy for developing therapeutic antibodies that achieve optimal activation of anti-tumor T cells.

Results

Characterisation and *in vitro* activity of a tetravalent anti-mouse CD27 antibody

To assess the impact of increased valency on anti-CD27 antibody potency, we engineered a tetravalent version of the anti-mouse (m) CD27 mAb AT124-1 by incorporating additional Fab arms into its structure (Figure 1A). Antibodies were produced as mouse IgG1 as this isotype is known to potentiate agonism by anti-TNFRSF antibodies in mice through FcγRII-mediated crosslinking [27-29]. To investigate the requirement for FcγR engagement for bivalent and tetravalent reagents, we also produced anti-mCD27 antibodies incorporating the N297Q (NQ) mutation which abrogates FcγR binding [30]. Size-exclusion chromatography (SEC) confirmed that all antibodies existed as monomers in solution, free from aggregates (Supplementary Figure 1A), and SDS-PAGE analysis established that heavy and light chains of the anticipated size were produced (Supplementary Figure 1B). The structure of tetravalent anti-mCD27 was also characterized by negative-staining electron microscopy. Class average image analysis revealed the tetrameric structure of the antibody, displaying four distinct Fab sections (Figure 1B). The outer Fab sections exhibited a degree of flexibility, consistent with the predicted mobility of the peptide linker connecting them to the inner Fab section (Figure 1B). Next, we employed surface plasmon resonance (SPR) to investigate the effect of increased valency on the binding strength to mCD27. Our results demonstrated a > 5-fold increase in apparent affinity, primarily attributed to a slower dissociation rate of the tetravalent antibody from the receptor (Figure 1C and Table 1). We also investigated the effects of increased valency on the binding of anti-mCD27 antibodies to mCD27 expressed on the surface of Jurkat cells and observed a significant increase in avidity, as reflected by a ~100-fold decrease in the EC50 value for the tetravalent format (Figure 1D). Next, we assessed if increased valency and avidity translated into enhanced NF-κB activation, a key downstream signaling pathway of CD27 [31, 32]. When applied in solution neither bivalent nor tetravalent anti-mCD27 antibodies induced GFP expression in $mCD27^+$ Jurkat NF-κB-GFP reporter cells (Figure 2A, left panel). However, both formats induced NF-κB signalling when $mCD27^+$ reporter cells were co-cultured with Chinese hamster ovary (CHO) cells expressing mouse FcγRII (Figure 2A, right panel and 2B). Importantly, whereas at high concentrations (10-100 nM) the two formats stimulated similar levels of NF-κB activation, tetravalent anti-mCD27 was by far the most active at concentrations ranging from 0.001-1 nM (Figure 2A, right panel). The enhanced potency of tetravalent anti-mCD27 when compared to bivalent anti-mCD27 and the

requirement for Fc-mediated crosslinking was similarly observed when OT-I T cell proliferation under conditions of sub-optimal peptide stimulation was used as the read out for CD27 signaling (Figure 2C). Collectively, our *in vitro* data suggest that the combination of tetravalency and FcγRII binding produces a level of activation not achievable with bivalent antibodies.

Impact of valency and FcγRII binding on in vivo antigen-specific CD8$^+$ T cell responses and immunotherapy with anti-mCD27 antibodies

To explore the broader implications of our *in vitro* data, we initially compared the ability of bivalent and tetravalent anti-mCD27 antibodies to boost a CD8$^+$ T cell response *in vivo*. This was first addressed using adoptively transferred CD45.1$^+$ OT-I T cells and administration of ovalbumin 257-264 peptide ($OVA_{257-264}$) combined with either bivalent or tetravalent anti-mCD27 antibodies. Figure 3A-C demonstrates that tetravalent anti-mCD27 treatment led to significantly greater CD8$^+$ T cell expansion compared to bivalent anti-mCD27 or an isotype control. This enhanced T cell proliferation was sustained throughout the contraction phase. Moreover, the 'Fc silent' N297A variants of the bivalent and tetravalent anti-mCD27 antibodies did not induce significant CD45.1$^+$ CD8$^+$ T cell expansion, indicating that FcγR-crosslinking was required for activity of anti-CD27 antibodies *in vivo*, thus corroborating our *in vitro* findings. Of note, this enhanced in vivo activity of the tetravalent anti-CD27 mIgG1 could not be attributed to improved pharmacokinetics, as it exhibited a slightly shorter plasma half-life compared to its bivalent counterpart (Supplementary Figure 2).

Next, we compared the activity of anti-mCD27 antibodies in an immunotherapy setting wherein mice bearing a B16 melanoma variant that expresses OVA as a surrogate tumor antigen (B16-OVA), were treated with OVA and the antibodies indicated in Figure 4. Mice were then assessed for endogenous OVA-specific CD8$^+$ T cell expansion and tumor growth. Consistent with the OT-I T cell responses, tetravalent anti-mCD27 elicited the strongest endogenous OVA-specific CD8$^+$ T cell response surpassing that of the bivalent format, and this response was sustained throughout the sampling period (Figure 4A-C). This enhanced T cell response correlated with more effective tumor control by tetravalent anti-mCD27 (Figure 4D). In contrast, but in keeping with their muted OVA-specific CD8$^+$ T cell responses, the Fc-inert mAb did not elicit robust tumor control. These experiments confirm that the tetravalent anti-mCD27 antibody induced a stronger endogenous OVA-specific CD8$^+$ T cell response and improved tumor control; although, due to the aggressiveness of B16-OVA tumors and the likely emergence of OVA-loss variants [33], tumor growth was ultimately not fully prevented (Figure 4D and Supplementary Figure 3).

Next, we conducted experiments to compare bivalent and tetravalent anti-mCD27 antibodies in a second model, the BCL_1 lymphoma, which lacks an identified tumor-specific antigen, and in which CD27 agonism had previously been shown to elicit protective T cell responses [19, 22, 24, 34]. As the Fc inert anti-CD27 antibodies showed limited activity, we focussed on testing antibodies with functional mIgG1 Fc in this model. Bivalent anti-mCD27 provided modest protection from the BCL_1 tumor, increasing median survival from 16 days in the isotype control group to 39.5 days (Figure 5A), which was further increased with the tetravalent anti-mCD27 antibody with median survival increasing to 71.5 days (Figure 5A).

Given that BCL_1 lymphoma grows primarily in the spleen and FcγRII is abundantly expressed on both malignant and normal B cells [35], we next tested the tetravalent anti-mCD27 antibody in the CT26 colon carcinoma model, where FcγRII expression is absent from the tumor and limited to the tumor-infiltrating immune cells. CT26 tumors are known to exhibit heterogeneous responses to immunotherapy with anti-PD-1 antibodies, typically segregating into responders and non-responders [36]. We observed a similar pattern in mice bearing established CT26 tumors treated with anti-mCD27 antibodies. Strikingly, while the bivalent anti-mCD27 mIgG1 achieved a cure rate of only 50% among responders, the tetravalent anti-mCD27 antibody led to complete tumor regression in all responding mice, highlighting its superior therapeutic potential (Figure 5B-D). Moreover, administration of a cumulative dose of 660 µg, equivalent to ~ 30 mg/kg of tetravalent anti-mCD27, did not induce weight loss in mice, suggesting that the enhanced anti-tumor activity was not associated with increased toxicity (Supplementary Figure 4A). Furthermore, treatment with tetravalent anti-mCD27 mIgG1 did not increase alanine aminotransferase (ALT) or aspartate aminotransferase (AST) enzymatic activity in the blood, both of which are key indicators of liver toxicity (Supplementary Figure 4B).

To understand the cell types involved in the anti-tumor response exerted by tetravalent anti-mCD27, we profiled T cell subsets within the tumor. Data presented in Supplementary Figure 5 demonstrates that treatment with tetravalent anti-mCD27 induced an increase in both total and activated (4-1BB$^+$ and Granzyme B$^+$) CD8$^+$ T cells without impacting total CD4$^+$ or Foxp3$^+$ CD4$^+$ regulatory T cells. These data support the hypothesis that tetravalent anti-mCD27 exerts its effects through direct co-stimulation of CD8$^+$ T cells.

Tetravalency and FcγRIIB engagement synergize for optimal immune stimulation by anti-human CD27 antibody

To evaluate the clinical relevance of our findings, we explored whether increased valency and FcγRIIB interactions could potentiate the activity of anti-human (h) CD27 antibodies. To this end we produced the agonistic anti-hCD27 antibody, hCD27.15 [37], in a standard bivalent human IgG1 format and in a tetravalent configuration similar to the tetravalent anti-mCD27 antibody. Our previous work has shown that this clone recognises an epitope distinct from that targeted by the clinical antibody Varlilumab and binds to human CD27 with moderate affinity, exhibiting stronger stimulatory activity [38]. Furthermore, to assess the impact of different FcγR in mediating antibody crosslinking, bivalent and tetravalent anti-hCD27 antibodies were generated using either a wild-type hIgG1 backbone, a hIgG1 variant (V11) with a higher FcγRIIB and a lower FcγRI affinity [12], or a variant (NA) that has compromised binding to FcγRs. SEC analysis confirmed that all anti-hCD27 antibodies were monomeric in solution and free from aggregates (Supplementary Figure 6A). In addition, the overall structure of the tetravalent anti-hCD27 was verified by negative-staining electron microscopy (Supplementary Figure 6B). We also assessed whether the modified structure of the tetravalent anti-hCD27 antibody affected its thermal stability. Although the melting temperature was slightly reduced compared to the bivalent format (56.7 °C vs. 63.5 °C; Supplementary Table 1), this is still well above physiological temperatures and the standard accelerated storage temperature of 40 °C for biopharmaceuticals, including antibodies [39].

SPR analysis revealed that tetravalent anti-hCD27 mAb demonstrated enhanced avidity for hCD27, as evidenced by a ~2-fold increase in apparent affinity and slower dissociation kinetics compared to bivalent anti-hCD27 (Supplementary Figure 7A and Supplementary Table 2). Furthermore, the increased avidity of tetravalent anti-hCD27 antibodies was also apparent when binding to hCD27$^+$ Jurkat cells was analysed by flow cytometry, with more tetravalent anti-hCD27 antibody detected at lower concentrations (Supplementary Figure 7B). The agonistic potential of these anti-hCD27 antibodies was then assessed using hCD27$^+$ Jurkat-NF-κB-GFP reporter cells. While bivalent anti-hCD27 antibodies (hIgG1, NA, and V11) showed limited activity in the absence of FcγR crosslinking (Figure 6A, top panels), tetravalent anti-hCD27 antibodies were approximately 1000-fold more potent at inducing NF-κB activation than their bivalent counterparts, even in the absence of FcγRIIB (Figure 6A, top panels). Although both bivalent and tetravalent antibodies (hIgG1 and V11) showed enhanced activity in the presence of FcγRIIB$^+$ CHO cells, tetravalent anti-hCD27 antibodies demonstrated a significant potency advantage, ranging from 40- to 400-fold, compared to their bivalent counterparts, as evidenced by their lower EC50 values (Figure 6A, lower panels). We then sought to determine if tetravalency and physiological expression of FcγRIIB in peripheral blood mononuclear cells synergised in promoting T cell proliferation. Interestingly, the addition of bivalent and to a lesser extent tetravalent anti-hCD27 hIgG1

had a slightly detrimental effect on cell proliferation, likely due to T cell deletion through antibody engagement of activating FcγRs on blood mononuclear cells (Figure 6B, left panels). In contrast, both bivalent and tetravalent anti-hCD27 V11 antibodies were able to enhance T cell proliferation with the tetravalent format demonstrating superior potency, as reflected by lower EC50 values (Figure 6B, right panels). Moreover, the importance of FcγRIIB engagement was further substantiated by the loss of costimulatory activity of the tetravalent anti-hCD27 NA variant (Figure 6B, center panels). Thus, the synergistic effect of antibody tetravalency and FcγRIIB engagement is also evident in the human setting.

Tetravalency enhances hCD27 clustering, while FcγRIIB engagement promotes polarization and reduces internalization

The recently resolved structure of the CD27-CD27 ligand (CD70) complex, which comprises 3 receptor molecules bound to homotrimeric CD70, suggests that CD27 signalling is initiated through receptor clustering [40]. Moreover, ligand bound CD27 superclusters with a higher receptor density may form through disulfide-bond dimerization of CD27 in the cell membrane [40]. To explore the effects of antibody valency on the distribution of membrane anchored CD27, we cultured Jurkat cells expressing hCD27-GFP fusion protein with either bivalent or tetravalent anti-hCD27 hIgG1 V11 and visualised the distribution of receptors by confocal microscopy. Initially, we assessed antibody induced receptor clustering in the absence of FcγRs and showed that the increased valency afforded by tetravalent anti-hCD27 mAb induced significantly more clusters per cell than bivalent anti-hCD27 at concentrations from 0.1 to 100 nM (Figure 7A and B). Since the functional activity of tetravalent anti-hCD27 hIgG1 V11 was improved by FcγRIIB binding, we sought to understand how this affects CD27 distribution in the membrane. Therefore, hCD27-GFP$^+$ Jurkat cells were co-cultured with either hFcγRIIB$^+$ CHO cells or control CHO cells together with the tetravalent anti-hCD27 hIgG1 V11 antibody. Whereas CD27 clusters formed in the absence of FcγRIIB were randomly distributed and rapidly internalized within 20-30 minutes, those formed by tetravalent anti-hCD27 hIgG1 V11 in the presence of hFcγRIIB$^+$ CHO cells were localized to cell-cell contacts (Figure 7C) and persisted on the cell surface (Figure 7C and D). Finally, we addressed if hyper-crosslinking of tetravalent anti-hCD27 mAb with a secondary antibody recapitulates the stimulatory effects of FcγRIIB engagement. Using hCD27$^+$ Jurkat NF-κB-GFP reporter T cells, we found that hyper-crosslinking increased the stimulatory effects of soluble tetravalent anti-hCD27 as evidenced by the higher GFP signal and increased proportion of GFP$^+$ Jurkat cells (Figure 7E and F). Importantly, however, engagement of FcγRIIB by tetravalent anti-hCD27 provided even greater levels of

GFP (Figure 7E and F), demonstrating that capture of tetravalent anti-hCD27 by FcγRIIB-expressing cells synergises with antibody tetravalency to maximise CD27 signalling.

Discussion

The importance of the CD27-CD70 costimulatory pathway in human immunity is underscored by the immune dysregulation observed in individuals with biallelic mutations in the CD27 and CD70 genes that lead to the absence of protein expression [41-44]. These individuals often experience uncontrolled Epstein-Barr virus infection, severe infectious mononucleosis, lymphoproliferation and lymphoma, concomitant with impaired generation of memory B and T cells and defective effector $CD8^+$ T cell function. Moreover, studies in mice have shown that CD27 agonism can augment anti-tumor $CD8^+$ T cell responses when delivered in the form of monotherapy or in combination with immune checkpoint inhibition [19, 20, 22]. Despite the promising preclinical data, the clinical response to Varlilumab, a human IgG1 anti-CD27 antibody, has been underwhelming [25, 26], prompting further research to elucidate the underlying reasons. The archetypal TNFSF/TNFRSF complex organisation consisting of a trimeric ligand engaging 3 receptors necessitates appropriate consideration in the design of therapeutic agonists. Although soluble recombinant CD70 fusion proteins that retain activity have been produced, their development as drug modalities is confounded by the need to engineer highly oligomeric proteins, which typically exhibit low production yield and poor pharmacokinetics [34]. The classical bivalent nature of antibodies makes them sub-optimal as TNFRSF agonists and except for some rare antibodies that exhibit intrinsic agonistic activity, the majority are poor agonists without further engineering [7]. One approach to overcome this limitation is through inhibitory FcγRIIB mediated antibody crosslinking which is thought to mimic receptor oligomerization induced by membrane-anchored TNFSF ligands [8, 9, 13]. Alternatively, antibody engineering strategies, such as modulating affinity [10], promoting Fab-Fab [16] or Fc-Fc [45] interactions as well as restricting Fab conformational flexibility [17, 18, 46], have been explored to enhance the activity of soluble anti-TNFRSF antibodies. However, the extent to which these approaches can replace FcγRIIB-dependent crosslinking remains unclear. In this study we sought to address the role of valency and FcγR binding in driving agonism by anti-CD27 antibodies. Consistent with previous reports, we found that the agonistic activity of bivalent anti-mCD27 mIgG1 was dependent on FcγR-mediated crosslinking both *in vitro* (Figure 2) and *in vivo* (Figures 3 and 4). Although FcγR engagement was still required for agonism by the tetravalent anti-mCD27 antibody, the potency of agonism was significantly improved as determined by measurement of NF-κB activation, primary T cell proliferation and *in vivo* expansion of antigen-specific $CD8^+$ T cells (Figures 2-4). Importantly, the

enhanced agonistic activity conferred by tetravalency resulted in superior anti-tumor efficacy across three distinct tumor models (Figure 4 and 5). Notably, this increased therapeutic potency was not associated with observable adverse effects, as indicated by stable body weight measurements in treated mice throughout the study period (Supplementary Figure 4A), and the absence of elevated liver enzymes (ALT and AST) in the blood (Supplementary Figure 4B). Furthermore, analysis of tumor-infiltrating lymphocytes in the CT26 model revealed that treatment with tetravalent anti-mCD27 led to an increased frequency of activated $CD8^+$ T cells, with no detectable changes in $CD4^+$ T cells or regulatory T cells (Supplementary Figure 5). These findings support the notion that the anti-tumor activity of tetravalent anti-mCD27 involves direct co-stimulation of $CD8^+$ T cells. To explore the generalizability of this approach, we produced a tetravalent form of an anti-hCD27 antibody and engineered variants thereof that preferentially bind to different FcγRs. While bivalent anti-hCD27 displayed limited intrinsic agonistic activity in NF-κB reporter assays, the tetravalent format significantly enhanced this activity, regardless of FcγRIIB presence (Figure 6A). However, in the T cell proliferation assay, the superior potency of tetravalent anti-hCD27 was observed only with the V11 variant, which displays selectively enhanced binding to FcγRIIB [12] (Figure 6B). In fact, treatment with anti-hCD27 hIgG1, an isotype that exhibits a high activating to inhibitory FcγR binding ratio, resulted in a reduction in the proportion of proliferating T cells, consistent with the strong depletion properties of hIgG1 (Figure 6B). This finding is reminiscent of the profound decrease in circulating $CD4^+$ T cells seen in individuals following administration of anti-hCD27 hIgG1 [25, 26] and suggest that the unmodified hIgG1 backbone could limit the efficacy of anti-CD27 antibodies. Our combined analysis of antibody binding, imaging, and functional data indicates that the higher avidity and slower dissociation rate of tetravalent anti-CD27 antibodies facilitate efficient receptor clustering and enhanced stability of complexes compared to bivalent antibodies. Subsequent binding of the antibody-receptor complexes to FcγRIIB promotes cluster polarization to the cell-cell interface and reduces CD27 internalization resulting in an overall increase in the concentration of active receptors at the cell-cell interface. The reduction of CD27 internalization is likely to be significant as CD27 has been shown to undergo clathrin-mediated endocytosis and degradation after binding to its natural ligand, CD70 [47]. Furthermore, the inability of secondary antibody crosslinking to fully recapitulate the strong NF-κB activation observed in the presence of FcγRIIB expressing cells emphasizes the importance of FcγRIIB-mediated CD27 polarization to the cell-cell interface for optimal activation. Although trimerization of some TNFRSF members, such as TNFRI, is thought to be sufficient for transducing downstream signalling, others like CD40, CD30 and CD27 require additional oligomerization [34, 48-51]. For example, previous studies have shown that the binding of

soluble trimeric CD70 to CD27 drives limited downstream signaling, but this could be enhanced by hexamerization [34]. Interestingly, the activity of a hexameric CD70-Fc dimer of trimer protein was also improved by FcγRIIB binding, suggesting similarities in the mechanisms by which FcγRIIB promotes the activity of CD27 agonists [34]. It remains to be determined whether other receptors can mimic the function of FcγRIIB in enhancing CD27 agonism. Exploring alternative anchoring receptors could provide opportunities to fine-tune CD27 signaling and optimize therapeutic outcomes. For example, targeting receptors that are preferentially expressed in tumor or lymph node microenvironments could lead to activation of different T cell subsets. Given the limited clinical success of current CD27-targeted therapies, our findings highlight the potential of leveraging multivalency and selective FcγR binding to transform anti-CD27 agonists and therefore offer a promising avenue for the development of next-generation anti-CD27 therapies. Moreover, the same approach could be utilized to optimally agonise other members of the TNFRSF such as OX40, where a lack of activity and disappointing clinical efficacy have been observed [52-56].

Our findings underscore the therapeutic potential of the tetravalent antibody format, which demonstrated robust anti-tumor activity across multiple preclinical tumor models and outperformed its bivalent counterpart. While these results are promising, several considerations remain regarding the translational applicability and developability of higher-valency formats. In our studies, the tetravalent construct showed a modest reduction in plasma half-life and thermal stability relative to the bivalent format, which may warrant further optimisation during development. The increased structural complexity may also carry a higher risk of immunogenicity in clinical settings, though this remains to be formally assessed. An important question is whether alternative strategies to promote receptor clustering, such as biparatopic antibodies [57] that engage distinct epitopes on the same target *in trans* could achieve similar functional outcomes without the need for increased valency. These approaches could be evaluated alongside tetravalent formats to optimise the balance between efficacy, pharmacological properties, and manufacturability in future antibody development.

Methods

Mice

C57BL/6J (Charles River UK, Strain code: 027), Balb/c (Strain code: 028, Charles River UK) and OT-I transgenic (Tg) mice (Charles River France, strain code: 642), were purchased from Charles River and stock colonies maintained by the University of Southampton Biomedical Research Facility. For C57BL/6

mice, 54 female 8-12 week old mice were used. For Balb/c mice, 81 female 8-12 week old mice were used. For OT-I Tg mice, 20 female 8-12 week old mice were used. All mice were randomly assigned into experimental groups, with experimental and control animals co-housed. Mice were maintained on a 12-hour light and dark cycle, an ambient temperature of 20-24, 55 % humidity ± 15 %, with food and water ad libitum. Mice were kept under specific pathogen free (SPF) conditions. Daily checks were performed to ensure mice remained healthy and environmental enrichment was provided. Mice were euthanised by CO_2 inhalation or cervical dislocation. All experiments were conducted following University of Southampton ethical approval and in accordance with the Animals (Scientific Procedures) Act 1986 as set out in PPL: P4D9C89EA and PIL: I66C5D543.

CD45.1 OT-I Tg adoptive transfer

To assess antigen-specific responses *in vivo*, splenocytes from OT-I Tg CD45.1 mice (n=20) containing $1x10^4$ $CD8^+$ T cells were adoptively transferred into C57BL/6J mice. After 24 hours, mice were intravenously challenged with a single dose of 30 nmole $OVA_{257-264}$ peptide and 200 µg of antibody. Antigen-specific T cell expansion was measured by peripheral blood sampling and identifying CD45.1 $CD8^+$ T cells by flow cytometry, at the time points indicated in Figure 3.

Tumor models

B16-OVA cells ($2x10^5$) were subcutaneously injected into the flank of C57BL/6j (n=48, 8-12 week old females) mice on day 0. Twenty-four hours later, mice were intravenously injected with a single dose of 5 mg Ovalbumin (Sigma, A5503) and a molar equivalent quantity (1.33 nmol) of bivalent or tetravalent anti-mCD27 antibody. Antigen-specific T cell expansion was measured by peripheral blood sampling and detection of $OVA_{257-264}$-MHC H2-K^b $tetramer^+$ $CD8^+$ T cells by flow cytometry, at the time points indicated in Figure 4. Tumor growth was monitored every 2-3 days by calliper and mice euthanised when cross-sectional area reached 225 mm^2. This is below the maximum allowed volume of 4000 mm^3, equivalent to 400 mm^2. For the BCL_1 lymphoma model [19, 58], $5x10^6$ tumor cells obtained from *in vivo* passage were intravenously injected into Balb/c mice (n=30, 8-12 week old females) on day 0, and a molar equivalent quantity of bivalent or tetravalent anti-mCD27 antibody (0.5 nmol) was injected intravenously on day 4, as a single dose. Tumour growth was monitored every 2-3 days by splenic palpation, with humane endpoint of gross splenomegaly where the spleen is enlarged and extended, weighing approximately 500-1000 mg. Survival period to the humane end point was plotted using the Kaplan-Meier method with analysis for significance by the log-rank (Mantle-Cox) test. CT26 cells ($5x10^5$)

were subcutaneously injected into the hind flank of Balb/c mice (n=29, 8-12 week old females) on day 0, and a molar equivalent of isotype mIgG1, bivalent anti-mCD27 mIgG1 or tetravalent anti-mCD27 mIgG1 (0.66 nmol) was injected on days 10, 13, 16 and 20. Mouse weight was monitored after the first antibody injection. Tumor growth was monitored every 2-3 days by caliper and mice euthanised when cross-sectional area reached 225 mm^2. This is below the maximum allowed volume of 4000 mm^3, equivalent to 400 mm^2. Survival period to the humane end point was plotted using the Kaplan-Meier method with analysis for significance by the log-rank (Mantle-Cox) test. For all tumor experiments, early termination was carried out if mouse welfare was deemed compromised, in accordance with the guidelines proposed by Foltz and Cullere [59].

CT26 tumor harvest

CT26 cells ($5x10^5$) were subcutaneously injected into the hind flank of Balb/c mice (n=10, 8-12 week old females) on day 0, and a molar equivalent of isotype mIgG1 or tetravalent anti-mCD27 mIgG1 (0.66 nmol) was injected on days 10 and 13. Mice were euthanised on day 16 and tumors were excised. Tumors were then diced, incubated with 50 µg/ml DNase I (Roche, 4716728001) and 0.5 WU/ml Liberase DL (Merck, LIBDL-RO) for 30 mins at 37 °C. Digestion was inhibited using cRPMI supplemented with 10 mM EDTA (Fisher Scientific, S311-100) and 20 mM HEPES (Gibco, 15630080). Tumor was then passed through a 70 µm cell strainer (Falcon, 352350), and cells were subsequently stained as specified for flow cytometry.

Antibody bioavailability

200 µg of specified antibody was injected intravenously into C57BL/6 mice (n=6, 8-12 week old females) on day 0, with blood sampling occurring on days 1, 3 and 7. Serum concentration was determined by ELISA, as previously reported [34]. Briefly, mCD27-ECD-hFc (R&D systems) was used as a capture reagent and bound anti-mCD27 antibodies detected using horseradish peroxidase-conjugated goat anti-mouse IgG.

Alanine aminotransferase (ALT) and aspartate aminotransferase (AST) detection assay

Balb/c mice (n=12, 8-12 week old females) were intraperitoneally injected with PBS or 200 µg of bivalent anti-mCD27 mIgG1 or tetravalent anti-mCD27 mIgG1 on day 0. Blood sampling was performed on days 3 and 7, after which samples were allowed to clot overnight at 4 °C. Serum was then assessed for ALT and AST enzymatic activity using an ALT activity assay (Sigma, MAK052) and AST activity assay (Sigma, MAK055), respectively. The activity assays were performed as per the manufacturers' instructions.

Cell Culture

The Jurkat NF-κB reporter T cell line (Jurkat NF-κB GFP, System Biosciences, TR850A-1), CHO-k1 cells (ATCC, CCL-61) and CT26 colon carcinoma (ATCC, CRL-2638) were grown in Roswell Park Memorial Institute (RPMI) medium 1640 (Gibco, 11875093), supplemented with 10 % v/v Foetal Bovine Serum (FBS, Sigma, F9665), 2 mM L-Glutamine (Gibco, 25030081), 1 mM Sodium Pyruvate (Gibco, 11360070), 100 U/ml Penicillin (Sigma, P4333-100ML), 100 µg/ml Streptomycin (Sigma, P4333) (cRPMI). Jurkat cells expressing hCD27-GFP and Jurkat NF-κB GFP mCD27 reporter cells were described previously [34, 38]. CHO hFcγRIIB (provided by Dr Robert Oldham) and CHO mFcγRII cell lines (provided by Dr Hannah Smith) were cultured in cRPMI containing 1 mg/ml geneticin (Gibco, 10131027). Jurkat NF-κB GFP hCD27 cells [38] were cultured in cRPMI containing 5 µg/ml puromycin (InVivoGen, ant-pr-1). B16-OVA (provided by Dr Caetano Reis e Sousa) were grown in complete Dulbecco's Modified Eagle Medium (DMEM, Gibco), supplemented with 10 % v/v FBS, 2 mM L-Glutamine, 1 mM Sodium Pyruvate, 100 U/ml Penicillin, 100 µg/ml Streptomycin.

Antibodies

The sequences of the anti-mCD27 and anti-hCD27 (hCD27.15) antibodies were derived from the AT124-1 hybridoma [19, 34] and US patent 9527916, respectively, and recombinant antibodies were produced as described previously [10, 34]. To produce tetravalent antibodies, additional V_H-C_H1 domains were encoded in the antibody cDNA, linked to the N-terminus of the heavy chain by a 2(GGGGS) linker. All antibody preparations were endotoxin low (< 5 EU endotoxin/mg) as determined using the Endosafe-PTS portable test system (Charles River Laboratories).

Flow cytometry

Fluorescently labelled antibodies were purchased from eBioscience: allophycocyanin (APC)-labelled or PerCP-Cyanine 5.5-labelled anti-mCD8α (53-6.7), APC-eF780-labelled anti-mCD45.2 (104), R-phycoerythrin (PE)-labelled anti-mFoxP3 (FJK-16s), Fluorescein isothiocyanate (FITC)-labelled anti-mCD4 (GK1.5), eFluor450 (eF450)-labelled anti-mCD45.1 (A20), eF450-labelled anti-hCD3 (UCHT1), eF450-labelled anti-m4-1BB (17B5), eF506-labelled anti-hCD4 (RPA-T4); or Biolegend: PE-Cyanine 7-labelled anti-hCD8α (RPA-T8), Alexa Fluor 647-labelled anti-granzyme B (GB11). $OVA_{257-264}$-specific T cells were identified with PE-labelled H2-K^b $OVA_{257-264}$ tetramer, produced in house. Fluorescently labelled secondary $F(ab)_2$ antibodies were purchased from Jackson ImmunoReasearch: allophycocyanin (APC)-labelled AffiniPure goat anti-mouse Fcγ fragment, APC-labelled AffiniPure goat anti-human Fcγ

fragment. If samples contained erythrocytes, these were first lysed using ACK buffer. Viability staining was performed with Fixable Viability Dye eFluor 506 (eBioscience) as per the manufacturers' instructions. FcγR-blocking was then performed with either 10 µg/ml anti-FcγRII/III (2.4G2, produced in house) or 10 % human AB serum (for human cells), at 4 °C for 10 mins, prior to a 30 min, 4 °C incubation with surface staining antibodies. If secondary detection with $F(ab)_2$ was used, the cells were washed after surface staining and then incubated with the secondary $F(ab)_2$ for 20 mins at 4 °C. For intracellular staining, cells were fixed and permeabilised using the FoxP3/Transcription Factor Staining Kit, as per the manufacturers' instructions (eBioscince, 00-5523-00). All antibodies and dilutions used are listed in Supplementary Tables 3 and 4. Cells were then washed before analysis on a BD FACS Canto II or a BD FACS Calibur using the BD FACSDiva software or BD CellQuest software, respectively.

Negative stain electron microscopy (EM)

Glow discharged carbon coated copper grids (300 mesh, TAAB Laboratories, C267/050) were floated on a droplet of antibody on parafilm, containing 1-5 µg/ml of tetravalent anti-CD27 antibody diluted in H_2O, for 1 min. The grids were then briefly floated on a drop of H_2O and then a drop of 1 % w/v uranyl acetate. Finally, the grids were floated on 1 % uranyl acetate (Electron Microscopy Sciences, 22400) for 30 seconds before blotting on filter paper and air-drying overnight. Images were captured using a transmission electron microscope (Hitachi HT7700, Voltage: 100 kV, magnification: 70,000). Class averages were generated using RELION v3.1.3 (Sjors Scheres, MRC Laboratory of Molecular Biology). In brief, micrographs were uploaded to RELION, which auto-selected particles in a template free manner using the Laplacian of Gaussian method. Particles then underwent 2D classification into class averages, with averages selected that were well resolved and contained real particles. 2D classification was repeated to refine class averages into recognisable tetravalent antibodies, with representative class averages selected.

SPR

The apparent affinity of antibodies for their target proteins was analysed using a Biacore T200 (Biacore). The target protein was captured using an anti-hFc or anti-his antibody that had been amine coupled to a CM5 chip (Cytiva, 29104988), as per the manufacturers' instructions. Target proteins were mCD27 ECD-hFc (R&D Systems, 574-CD-050) or hCD27 ECD-Fc-his (R&D Systems, 382-CD-100); as indicated in Figure 1 and Supplementary Figure 7. The amount captured was optimised for each receptor. Antibodies diluted in HBS-EP+ (Cytiva, BR100669) to the concentrations indicated in Figure 1 and Supplementary

Figure 7 were injected into the flow cell at 30 µl/min for 300 s, to allow the antibodies to associate to the target protein. HBS-EP+ buffer was then injected into the flow cells at 30 µl/min to allow the antibody to dissociate, before the chip was regenerated with 3 M $MgCl_2$ at 20 µl/s for 1 min. Kinetics were then assessed in the Biacore Kinetics v3 software.

SDS PAGE and SEC

Protein samples (1-2 µg) were incubated with reducing Lammeli buffer containing additional SDS (62.5 mM Tris pH 6.5 (Sigma, 20-160), 4 % w/v SDS (VWR chemicals, 44215HN), 10 % v/v glycerol (Sigma, G9012), 0.04 % v/v bromophenol blue (VWR Chemicals, BDH7392-2) and 62.5 mM DTT (R0861)) for 30 min at ambient temperature. Protein samples were boiled for 5 min and then loaded onto a 10 % Bolt Bis-Tris Gel (Invitrogen, NW00100BOX) and separation was performed at 100 V for 15 minutes and then 140 V for 1 hour. The gel was fixed using 10 % acetic acid (VWR Chemicals) and 25 % isopropanol (Fisher Scientific, 10173240) and then stained with 60 mg/L Brilliant Blue (Sigma, B0770) in 10% acetic acid. Excess Coomassie Blue staining was removed by multiple washes with 10% acetic acid on a rocker for 30 minutes to 1 hour. The gel was imaged using the UVP BioSpectrum AC Imaging System (UVP). Antibodies (20-40 µg/sample) were assessed by analytical SEC using a Zorbax GF-250 column (Agilent) and a 0.2M phosphate running buffer pH 7.0 containing 1M dimethyl formamide, at a flow rate of 0.4 ml/min.

Nano differential scanning fluorimetry

PBS control and antibodies (1 mg/ml in PBS) were loaded into the Prometheus NT.48 (NanoTemper technologies). The temperature was increased from 14 °C to 95 °C at 1 °C per minute, with intrinsic protein fluorescence collected at 330 nm and 350 nm. Unfolding temperature was calculated by PR ThermControl software (NanoTemper technologies) using the first derivative of the 350/330 nm fluorescence.

Jurkat NF-κB GFP activation

The Jurkat NF-κB GFP reporter cell lines (System Biosciences) expressing either mCD27 [34] or hCD27 [38] were described previously. To investigate NF-κB activation, cells were incubated with anti-CD27 antibodies for 5 hours at 37 °C and either untransfected, mFcγRII transfected (provided by Dr Hannah Smith) or hFcγRIIB transfected CHO cells (provided by Dr Robert Oldham). GFP production was detected by flow cytometry.

Mouse T cell proliferation

Splenocytes 2x10^5/well from OT-I Tg C57BL/6 mice were stimulated with 1 pM $OVA_{257-264}$ peptide (Peptide synthetics, 47874) and anti-mCD27 antibodies or an isotype control. Cells were incubated at 37 °C, 5 % CO_2 for 48 hours before 1 µCi of ^{3}H-thymidine was added to each well for 16 hours. Cells were then lysed, with lysates transferred to filter plates (Opti-plate-96, Perkin Elmer, 101687-172). 40 µl/well Scintillant fluid (Perkin Elmer) was then added before incorporation of ^{3}H-thymidine was measured by scintillation counting (TopCount).

Human T cell proliferation

Human PBMCs were isolated from anonymised leukocyte cones from healthy adult donors through the NHS blood and transplant service. The use of human tissue was approved by the East of Scotland Research Ethics Service, Tayside, UK and via the Faculty of Medicine Research Ethics Committee under submission 19660. PBMCs were isolated from leukocyte cones by density gradient centrifugation using Lymphoprep (Stemcell, 18060). Isolated PBMCs were labelled with 2 µM CFSE (ThermoFisher Scientific, C34554) for 10 mins. CFSE-labelled PBMCs 1x10^5/well were stimulated with 0.1 ng/ml anti-hCD3 (OKT3) and 0.1-10 nM of anti-hCD27 antibodies or isotype control as indicated in Figure 6. CFSE dilution in $CD4^+$ and $CD8^+$ T cells was measured after 96 hours by flow cytometry. CFSE low cells were identified by comparison to CFSE labelled cells that were cultured in the absence of any stimulation.

Clustering confocal microscopy

Jurkat cells (1.5 x10^5) expressing hCD27-GFP fusion protein [38] were stimulated with either bivalent or tetravalent anti-hCD27 antibodies at the concentrations indicated in Figure 7 in a final volume of 200 µl in a 96-well U-bottomed plate at 37 °C for 10 mins. The cells were then fixed with 4 % PFA for 20 mins before imaging on a poly-D-lysine (Gibco, A3890401) coated µ-slide 18 well microscopy chamber (Ibidi, 81811). Cells were imaged in confocal mode (exposure: 3000 ms; line spacing: 2; 100x objective lens) using an ONI Nanoimager (ONI), before analysis with NimOS v1.18 and ImageJ. Clusters were defined as regions of membrane that had a fluorescence intensity above 15000, which was determined using the threshold setting on ImageJ (ImageJ).

Cell-cell clustering

Untransfected or hFcγRIIB$^+$ CHO cells (10^4) were labelled with CellTracer far red (Invitrogen, C34564), as per the manufacturers' instructions, and the cells plated onto a poly-D-lysine coated µ-slide 18 well microscopy chamber and incubated at 37 °C in 5 % CO_2 overnight. Jurkat hCD27-GFP cells (3x10^4) and antibodies (1 nM) were added to the wells for 10-30 minutes (as indicated in Figure 7) before fixing with

4 % PFA (ThermoFisher Scientific, 28908) for 20 mins. The cells were imaged in confocal mode (488 laser: exposure: 3000 ms, line spacing: 2; 647 laser: exposure: 150 ms, line spacing: 2; 100x objective lens) using an ONI Nanoimager, before analysis with NimOS v1.18 and ImageJ. Internalisation was measured by selecting the intracellular region of the Jurkat hCD27-GFP cells as a region of interest (ROI) on ImageJ and then calculating the mean fluorescence intensity of the ROI.

Statistical analysis

GraphPad Prism 9 was used for statistical analysis. Ordinary one-way analysis of variance (ANOVA) with Tukey's post hoc multiple comparison test or a paired-t test was used as indicated in the figure legends throughout. Tumor area was analysed by calculating the area under the curve (AUC) before performing a one-way ANOVA. Where error bars are shown, they indicate SEM or SD as detailed in the figure legends. Survival analysis was performed using log-rank (Mantel-Cox) test between indicated groups. *p<0.05, **p<0.01, ***p<0.001, ****p<0.0001.

Data Availability

All data are included in the Supplementary Information or available from the authors, as are unique reagents used in this Article. The raw numbers for charts and graphs are available in the Source Data file whenever possible. Source data are provided with this paper.

Corresponding Author. Correspondence and material requests should be addressed to Prof Aymen Al-Shamkhani. Email: aymen@soton.ac.uk.

References

1. Esensten, J.H., et al., *CD28 Costimulation: From Mechanism to Therapy.* Immunity, 2016. **44**(5): p. 973-88.
2. Chen, L. and D.B. Flies, *Molecular mechanisms of T cell co-stimulation and co-inhibition.* Nat Rev Immunol, 2013. **13**(4): p. 227-42.
3. Hanahan, D. and R.A. Weinberg, *Hallmarks of cancer: the next generation.* Cell, 2011. **144**(5): p. 646-74.
4. Driessens, G., J. Kline, and T.F. Gajewski, *Costimulatory and coinhibitory receptors in anti-tumor immunity.* Immunol Rev, 2009. **229**(1): p. 126-44.
5. Sharma, P., et al., *Immune checkpoint therapy-current perspectives and future directions.* Cell, 2023. **186**(8): p. 1652-1669.
6. Townsend, S.E. and J.P. Allison, *Tumor rejection after direct costimulation of CD8+ T cells by B7-transfected melanoma cells.* Science, 1993. **259**(5093): p. 368-70.
7. Lim, S.H., et al., *Agonist Antibodies for Cancer Immunotherapy: History, Hopes, and Challenges.* Clin Cancer Res, 2024. **30**(9): p. 1712-1723.

8. White, A.L., et al., *Interaction with FcγRIIB Is Critical for the Agonistic Activity of Anti-CD40 Monoclonal Antibody.* The Journal of Immunology, 2011. **187**(4).
9. Yu, X., et al., *Complex Interplay between Epitope Specificity and Isotype Dictates the Biological Activity of Anti-human CD40 Antibodies.* Cancer Cell, 2018. **33**(4): p. 664-675 e4.
10. Yu, X., et al., *Reducing affinity as a strategy to boost immunomodulatory antibody agonism.* Nature, 2023. **614**(7948): p. 539-547.
11. Li, F. and J.V. Ravetch, *Inhibitory Fcgamma receptor engagement drives adjuvant and anti-tumor activities of agonistic CD40 antibodies.* Science, 2011. **333**(6045): p. 1030-4.
12. Mimoto, F., et al., *Engineered antibody Fc variant with selectively enhanced FcγRIIb binding over both FcγRIIaR131 and FcγRIIaH131.* Protein Engineering, Design and Selection, 2013. **26**(10).
13. Dahan, R., et al., *Therapeutic Activity of Agonistic, Human Anti-CD40 Monoclonal Antibodies Requires Selective FcgammaR Engagement.* Cancer Cell, 2016. **29**(6): p. 820-831.
14. Zhang, D., M.V. Goldberg, and M.L. Chiu, *Fc Engineering Approaches to Enhance the Agonism and Effector Functions of an Anti-OX40 Antibody.* J Biol Chem, 2016. **291**(53): p. 27134-27146.
15. Yang, Y., et al., *Tetravalent biepitopic targeting enables intrinsic antibody agonism of tumor necrosis factor receptor superfamily members.* mAbs, 2019. **11**(6).
16. Leonard, B., et al., *Antibody homotypic interactions are encoded by germline light chain complementarity determining region 2.* Proc Natl Acad Sci U S A, 2022. **119**(23): p. e2201562119.
17. Orr, C.M., et al., *Hinge disulfides in human IgG2 CD40 antibodies modulate receptor signaling by regulation of conformation and flexibility.* Sci Immunol, 2022. **7**(73): p. eabm3723.
18. Romei, M.G., et al., *i-shaped antibody engineering enables conformational tuning of biotherapeutic receptor agonists.* Nat Commun, 2024. **15**(1): p. 642.
19. French, R.R., et al., *Eradication of lymphoma by CD8 T cells following anti-CD40 monoclonal antibody therapy is critically dependent on CD27 costimulation.* Blood, 2007. **109**(11).
20. Roberts, D.J., et al., *Control of established melanoma by CD27 stimulation is associated with enhanced effector function and persistence, and reduced PD-1 expression of tumor infiltrating CD8(+) T cells.* J Immunother, 2010. **33**(8): p. 769-79.
21. He, L.Z., et al., *Agonist anti-human CD27 monoclonal antibody induces T cell activation and tumor immunity in human CD27-transgenic mice.* J Immunol, 2013. **191**(8): p. 4174-83.
22. Buchan, S.L., et al., *PD-1 Blockade and CD27 Stimulation Activate Distinct Transcriptional Programs That Synergize for CD8+ T-Cell–Driven Antitumor Immunity.* Clinical Cancer Research, 2018. **24**(10).
23. Guelen, L., et al., *Preclinical characterization and clinical translation of pharmacodynamic markers for MK-5890: a human CD27 activating antibody for cancer immunotherapy.* Journal for ImmunoTherapy of Cancer, 2022. **10**(9).
24. Wasiuk, A., et al., *CD27-Mediated Regulatory T Cell Depletion and Effector T Cell Costimulation Both Contribute to Antitumor Efficacy.* The Journal of Immunology, 2017. **199**(12).
25. Burris, H.A., et al., *Safety and Activity of Varlilumab, a Novel and First-in-Class Agonist Anti-CD27 Antibody, in Patients With Advanced Solid Tumors.* J Clin Oncol, 2017. **35**(18): p. 2028-2036.
26. Sanborn, R.E., et al., *Safety, tolerability and efficacy of agonist anti-CD27 antibody (varlilumab) administered in combination with anti-PD-1 (nivolumab) in advanced solid tumors.* Journal for ImmunoTherapy of Cancer, 2022. **10**(8).
27. White, A.L., et al., *Interaction with FcgammaRIIB is critical for the agonistic activity of anti-CD40 monoclonal antibody.* J Immunol, 2011. **187**(4): p. 1754-63.
28. Buchan, S.L., et al., *Antibodies to Costimulatory Receptor 4-1BB Enhance Anti-tumor Immunity via T Regulatory Cell Depletion and Promotion of CD8 T Cell Effector Function.* Immunity, 2018. **49**(5): p. 958-970 e7.

29. Wasiuk, A., et al., *CD27-Mediated Regulatory T Cell Depletion and Effector T Cell Costimulation Both Contribute to Antitumor Efficacy.* J Immunol, 2017. **199**(12): p. 4110-4123.
30. Liu, R., et al., *Fc-Engineering for Modulated Effector Functions—Improving Antibodies for Cancer Treatment.* Antibodies 2020, Vol. 9, Page 64, 2020. **9**(4).
31. Akiba, H., et al., *CD27, a member of the tumor necrosis factor receptor superfamily, activates NF-kappaB and stress-activated protein kinase/c-Jun N-terminal kinase via TRAF2, TRAF5, and NF-kappaB-inducing kinase.* J Biol Chem, 1998. **273**(21): p. 13353-8.
32. Ramakrishnan, P., W. Wang, and D. Wallach, *Receptor-specific signaling for both the alternative and the canonical NF-kappaB activation pathways by NF-kappaB-inducing kinase.* Immunity, 2004. **21**(4): p. 477-89.
33. Kaluza, K.M., et al., *Adoptive T cell therapy promotes the emergence of genomically altered tumor escape variants.* Int J Cancer, 2012. **131**(4): p. 844-54.
34. Dadas, O., et al., *Fcgamma receptor binding is required for maximal immunostimulation by CD70-Fc.* Front Immunol, 2023. **14**: p. 1252274.
35. White, A.L., et al., *Fcgamma receptor dependency of agonistic CD40 antibody in lymphoma therapy can be overcome through antibody multimerization.* J Immunol, 2014. **193**(4): p. 1828-35.
36. Sugiyarto, G., et al., *Reactivation of low avidity tumor-specific CD8(+) T cells associates with immunotherapeutic efficacy of anti-PD-1.* J Immunother Cancer, 2023. **11**(8).
37. Van Eenennaam, H., et al., *Agonistic antibody to CD27*. 2016, Aduro Biotech Holdings Europe B V.
38. Heckel, F., et al., *Agonistic CD27 antibody potency is determined by epitope-dependent receptor clustering augmented through Fc-engineering.* Commun Biol, 2022. **5**(1): p. 229.
39. Mieczkowski, C., et al., *Blueprint for antibody biologics developability.* MAbs, 2023. **15**(1): p. 2185924.
40. Liu, W., et al., *Structural delineation and phase-dependent activation of the costimulatory CD27:CD70 complex.* J Biol Chem, 2021. **297**(4): p. 101102.
41. van Montfrans, J.M., et al., *CD27 deficiency is associated with combined immunodeficiency and persistent symptomatic EBV viremia.* J Allergy Clin Immunol, 2012. **129**(3): p. 787-793 e6.
42. Izawa, K., et al., *Inherited CD70 deficiency in humans reveals a critical role for the CD70-CD27 pathway in immunity to Epstein-Barr virus infection.* J Exp Med, 2017. **214**(1): p. 73-89.
43. Abolhassani, H., et al., *Combined immunodeficiency and Epstein-Barr virus-induced B cell malignancy in humans with inherited CD70 deficiency.* J Exp Med, 2017. **214**(1): p. 91-106.
44. Ghosh, S., et al., *Extended clinical and immunological phenotype and transplant outcome in CD27 and CD70 deficiency.* Blood, 2020. **136**(23): p. 2638-2655.
45. Zhang, D., et al., *Functional optimization of agonistic antibodies to OX40 receptor with novel Fc mutations to promote antibody multimerization.* MAbs, 2017. **9**(7): p. 1129-1142.
46. White, A.L., et al., *Conformation of the human immunoglobulin G2 hinge imparts superagonistic properties to immunostimulatory anticancer antibodies.* Cancer Cell, 2015. **27**(1): p. 138-48.
47. Jaeger-Ruckstuhl, C.A., et al., *Signaling via a CD27-TRAF2-SHP-1 axis during naive T cell activation promotes memory-associated gene regulatory networks.* Immunity, 2024/02/13. **57**(2).
48. Schneider, P., et al., *Conversion of membrane-bound Fas(CD95) ligand to its soluble form is associated with downregulation of its proapoptotic activity and loss of liver toxicity.* J Exp Med, 1998. **187**(8): p. 1205-13.
49. Haswell, L.E., M.J. Glennie, and A. Al-Shamkhani, *Analysis of the oligomeric requirement for signaling by CD40 using soluble multimeric forms of its ligand, CD154.* Eur J Immunol, 2001. **31**(10): p. 3094-100.
50. Hargreaves, P.G. and A. Al-Shamkhani, *Soluble CD30 binds to CD153 with high affinity and blocks transmembrane signaling by CD30.* Eur J Immunol, 2002. **32**(1): p. 163-73.

51. Kucka, K. and H. Wajant, *Receptor Oligomerization and Its Relevance for Signaling by Receptors of the Tumor Necrosis Factor Receptor Superfamily.* Front Cell Dev Biol, 2020. **8**: p. 615141.
52. Glisson, B.S., et al., *Safety and Clinical Activity of MEDI0562, a Humanized OX40 Agonist Monoclonal Antibody, in Adult Patients with Advanced Solid Tumors.* Clin Cancer Res, 2020. **26**(20): p. 5358-5367.
53. Gutierrez, M., et al., *OX40 Agonist BMS-986178 Alone or in Combination With Nivolumab and/or Ipilimumab in Patients With Advanced Solid Tumors.* Clin Cancer Res, 2021. **27**(2): p. 460-472.
54. Diab, A., et al., *A Phase I, Open-Label, Dose-Escalation Study of the OX40 Agonist Ivuxolimab in Patients with Locally Advanced or Metastatic Cancers.* Clin Cancer Res, 2022. **28**(1): p. 71-83.
55. Kim, T.W., et al., *First-In-Human Phase I Study of the OX40 Agonist MOXR0916 in Patients with Advanced Solid Tumors.* Clin Cancer Res, 2022. **28**(16): p. 3452-3463.
56. Postel-Vinay, S., et al., *First-in-human phase I study of the OX40 agonist GSK3174998 with or without pembrolizumab in patients with selected advanced solid tumors (ENGAGE-1).* J Immunother Cancer, 2023. **11**(3).
57. Niquille, D.L., K.M. Fitzgerald, and N. Gera, *Biparatopic antibodies: therapeutic applications and prospects.* MAbs, 2024. **16**(1): p. 2310890.
58. Warnke, R.A., et al., *The pathology and homing of a transplantable murine B cell leukemia (BCL1).* J Immunol, 1979. **123**(3): p. 1181-8.
59. Ullman-Cullere, M.H. and C.J. Foltz, *Body condition scoring: a rapid and accurate method for assessing health status in mice.* Lab Anim Sci, 1999. **49**(3): p. 319-23.

Acknowledgements. We thank Dr Hannah Smith and Dr Robert Oldham for the kind gift of CHO cells expressing FcγRs. We would like to acknowledge that the purchase of the Nanoimager used in our microscopy studies was made possible by a kind gift from the Mark Benevolent Fund. We are grateful to members of the Biomedical Research Facility, University of Southampton for their help with the murine *in vivo* studies. The study was funded by Cancer Research UK Award number DRCDDRPGMApr2020\100005 (AAS, SAB, MSC).

Author contributions. M.A.W. performed and analyzed the experiments with the help of A.P, H.J.M., S.G.B., H.T.C.C., T.I., C.A.P., C.I.M. and S. J. A.Al-S. conceived the project. A.Al-S., S.A.B., and M.S.C. supervised the project. M.A.W. and A.AL-S. wrote the manuscript with feedback from M.S.C., S.A.B. and S.H.L.

Competing interests. A.A-S and S.H.L are inventors on patents pertaining to the generation and therapeutic use of agonist anti-CD27 antibodies and have received research funding from Celldex Therapeutics in relation to anti-CD27 antibodies. The remaining authors declare no competing interests.

Tables

Antibody	K_a	K_d	Apparent affinity

	($x 10^6 M^{-1}s^{-1}$)	($x 10^{-3} s^{-1}$)	(K_D, $x 10^{-9}$ M)
Anti-mCD27 mIgG1	**1.3**	**12.7**	**9.5**
Anti-mCD27 mIgG1 NQ	**1.1**	**14.4**	**13.1**
Tetra anti-mCD27 mIgG1	**1.6**	**2.9**	**1.8**
Tetra anti-mCD27 mIgG1 NQ	**1.6**	**2.4**	**1.5**

Table 1: Summary of the binding kinetics of anti-mCD27 antibodies.

Kinetic fits for anti-mCD27 antibody binding were calculated using the Biacore kinetics summary v3.1 software and the bivalent (2:1) binding model fit to the data in Figure 1C. Source data are provided as a Source Data file.

Figure Legends

Fig. 1: Tetravalency enhances anti-mCD27 avidity for mCD27.

a Schematic representation of the tetravalent (Tetra) antibody, with CDRs indicated in red. **b** Representative class averages (n=49, 68, 50 and 42 per image) from negative stain electron microscopy of Tetra anti-mCD27. **c** SPR analysis of anti-mCD27 antibodies. The indicated antibodies were injected over immobilised mCD27-Fc for 300s at a starting concentration of 3.7 nM and then a 3-fold serial dilution thereof. Data show concentrations from one experiment. **d** $mCD27^+$ Jurkat cells were stained with anti-mCD27 antibodies with bound antibody detected using an APC-conjugated anti-mouse Fc secondary $F(ab)_2$. Secondary antibody binding was detected using flow cytometry. Data points are the mean ± SEM (n=3) from 3 independent experiments. Source data are provided as a Source Data file.

Fig. 2: Tetravalent anti-mCD27 induces potent agonism in the presence of mFcγRII.

a, b $mCD27^+$ Jurkat NF-κB GFP reporter cells were co-cultured with either wild-type (WT CHO) or $mFc\gamma RII^+$ CHO cells in the presence of the indicated antibodies. NF-κB activation was quantitated by GFP expression

using flow cytometry. **a** GFP production from Jurkat cells after co-culture with WT CHO cells (left panel) or mFcγRII$^+$ CHO cells (right panel) at the indicated antibody concentrations. Data points are the mean ± SEM (n=3) from 3 independent experiments. Statistical significance was determined by one-way ANOVA (Tetra anti-mCD27 mIgG1 versus anti-mCD27 mIgG1), with significance values indicated in figure. **b** Representative histograms of GFP production at 1 nM of the indicated antibodies when mCD27$^+$ Jurkat NF-κB GFP cells were co-cultured with mFcγRII$^+$ CHO cells. **c** Naïve splenocytes were stimulated with $OVA_{257-264}$ peptide in the presence of the indicated antibodies for 72 hours. T cell proliferation was assessed by measuring the incorporation of ^{3}H-thymidine for the final 16 hours of culture. Each data point is the mean of triplicate measurements. Bars are the mean ± SEM (n=4) from 4 independent experiments, except Isotype control mIgG1 at 10 and 0.1 nM, which show mean ± SEM (n=2) from 2 independent experiments. Statistical significance was determined by one-way ANOVA with Tukey's post-hoc test for multiple comparisons and significance values indicated in figure. Responses of 'NQ' antibody variants were not statistically significant compared to the isotype control. Source data are provided as a Source Data file.

Fig. 3: Optimal priming of antigen specific CD8$^+$ T cells by anti-mCD27 requires tetravalency and FcγR engagement.

a-c C57BL/6 mice received OT-I Tg CD45.1$^+$ cells on day 0 followed by $OVA_{257-264}$ peptide and the indicated antibodies on day 1. Expansion of $OVA_{257-264}$ specific CD45.1$^+$ CD8$^+$ T cells was monitored by flow cytometry of peripheral blood samples following staining with anti-CD8 and anti-CD45.1. **a** Representative flow cytometry contour plots obtained on day 5 and **b** the compiled data with each bar representing the mean ± SEM from 4 individual mice from one experiment (n=4 mice per group). Statistical significance was determined by one-way ANOVA, with Tukey's post-hoc test for multiple comparisons and significance values indicated in figure. **c** Time course of CD45.1$^+$ CD8$^+$ T cell expansion. Data points are the mean ± SEM from 4 individual mice from one experiment (n=4 mice per group). Statistical significance was assessed by one-way ANOVA with Tukey's post-hoc test for multiple comparisons on areas under the curve (AUC), with significance values indicated in figure. Responses of 'NQ' antibody variants were not statistically significant compared to the isotype control. Source data are provided as a Source Data file.

Fig. 4: Tetravalent anti-mCD27 generates superior vaccine responses compared to its bivalent counterpart.

a-d C57BL/6 mice were inoculated with s.c. B16-OVA melanoma on day 0 and treated with OVA and the indicated antibodies on day 1. Expansion of endogenous antigen-specific $CD8^+$ T cells was monitored by obtaining peripheral blood samples on from day 0 to day 12 and staining with anti-CD8 and H2-K^b - $OVA_{257-264}$ tetramer (tetramer$^+$). **a-b, a** representative .flow cytometry contour plots and **b** compiled data of the antigen-specific T cell response on day 7 with each bar representing the mean ± SEM from 12 individual mice (n=12, isotype mIgG1, anti-mCD27 mIgG1, tetra anti-mCD27 mIgG1) across 2 independent experiments or 6 individual mice (n=6, anti-mCD27 mIgG1 NQ, tetra anti-mCD27 mIgG1 NQ) from 1 experiment. Statistical significance was determined using one-way ANOVA, with Tukey's post-hoc test for multiple comparisons and significance values indicated in figure. **c** Time course of the antigen-specific T cell response with each data point representing the mean ± SEM (n=12, isotype mIgG1, anti-mCD27 mIgG1, tetra anti-mCD27 mIgG1; n=6, anti-mCD27 mIgG1 NQ, tetra anti-mCD27 mIgG1 NQ). Statistical significance was determined by calculating the AUC and performing one-way ANOVA on AUC values, with significance values indicated in figure. **d** Tumor area for mice inoculated with B16-OVA cells on day 0 and treated with OVA and the indicated antibodies on day 1. Data points are the mean ± SEM of 12 individual mice (n=12, isotype mIgG1, anti-mCD27 mIgG1, tetra anti-mCD27 mIgG1) across 2 independent experiments or 6 individual mice (n=6, anti-mCD27 mIgG1 NQ, tetra anti-mCD27 mIgG1 NQ) from 1 experiment. Statistical significance by one-way ANOVA was performed on AUC, with significance values indicated in figure. Responses of 'NQ' antibody variants were not statistically significant compared to the isotype control. Source data are provided as a Source Data file.

Fig. 5: Tetravalent anti-mCD27 generates superior anti-tumor responses compared to its bivalent counterpart.

a Percentage survival to the humane end-point of Balb/c mice inoculated with BCL_1 lymphoma and treated with the indicated antibodies on day 4. Data shown are from 10 mice across 2 independent experiments (n=10 mice per group). **b** Individual tumor growth curves of Balb/c mice inoculated with CT26 colon carcinoma and treated with the indicated antibodies on days 11, 13, 16, 18. Data shown are from 9 mice (Isotype mIgG1) or 10 mice (anti-mCD27 mIgG1 and tetra anti-mCD27 mIgG1) across 2 independent experiments, with non-responders shown in blue and responders shown in purple. **c** Summary of tumor growth data from responding and isotype control mice shown in **b** calculated as the group mean AUC of Isotype mIgG1 (n=9), anti-mCD27 mIgG1 (n=6) or tetra anti-mCD27 mIgG1 (n=5) with error bars indicating SD. **d** Percentage survival of CT26-bearing mice in **b** to the humane end-point. Statistical significance was determined by Log-rank (Mantel-Cox) test (**a** and **d**), two way ANOVA (**b**), or one way

ANOVA (**c**), with significance values indicated in figure. For analysis of statistical significance by ANOVA, Tukey's post-hoc test was used for multiple comparisons. Source data are provided as a Source Data file.

Fig. 6: Tetravalency and FcγRIIB engagement synergize for optimal stimulation of human CD27.

a hCD27$^+$ Jurkat NF-κB GFP reporter cells were co-cultured with either WT CHO or hFcγRIIB$^+$ CHO cells in the presence of the indicated antibodies. NF-κB activation was quantitated by GFP expression using flow cytometry. **a** GFP production from Jurkat cells after co-culture with WT CHO cells (above) or hFcγRIIB$^+$ CHO cells (below) and the specified antibodies; hIgG1 (left), hIgG1 NA (centre) or hIgG1 V11 (right). Data points are the mean ± SEM (n=3) from 3 independent experiments. Statistical significance was determined by one-way ANOVA (Tetra anti-hCD27 versus anti-CD27 IgG), with significance values indicated in figure. **b** Human CFSE-labelled PBMCs were stimulated with sub-optimal anti-CD3 and the indicated antibodies, hIgG1 (left), hIgG1 NA (centre) or hIgG1 V11 (right). CD8$^+$ (above) and CD4$^+$ (below) T cell proliferation was assessed by CFSE dilution with CFSE low cells identified by comparison to cells that were cultured in the absence of any stimulation. Each data point is the mean ± SEM (n=5) from 5 independent experiments across 5 different donors. Statistical significance between bivalent anti-CD27 and bivalent isotype control (coloured numbers) and tetravalent anti-CD27 and tetravalent isotype control (black numbers) was determined by one-way ANOVA, with significance values indicated in figure. Source data are provided as a Source Data file.

Fig. 7: Tetravalent anti-hCD27 hIgG1 V11 induces greater cluster formation, with FcγRIIB engagement polarizing hCD27 clusters and reducing internalization.

a, b Jurkat cells expressing hCD27-GFP$^+$ fusion protein were stimulated with the specified antibodies at the indicated concentrations, before PFA fixation and confocal imaging. **a** Representative images at 100 nM (white corresponds to hCD27–GFP fluorescence; clustered areas of the signal are indicated by green arrows) and **b** quantification of the number of clusters per cell section, performed using ImageJ. Data shown are mean ± SEM of CD27 clusters per cell section from 2 independent experiments (n=54 cells). Statistical significance was determined by one-way ANOVA, with significance values indicated in figure. **c, d** hCD27-GFP$^+$ Jurkat cells were stimulated with 1 nM tetra anti-hCD27 hIgG1 V11 and either WT CHO cells or hFcγRIIB$^+$ CHO cells for the specified time points before PFA fixation and confocal imaging using Oxford Nanoimager. **c** Representative images of hCD27-GFP$^+$ Jurkat cells with WT CHO (upper panels) or hFcγRIIB$^+$ CHO (lower panels) for the specified timepoints. Dashed blue and green lines (determined by brightfield and confocal images) indicate the plasma membrane of CHO and Jurkat cells,

respectively. **d** Quantification of intracellular GFP MFI of individual cell sections of hCD27-GFP$^+$ Jurkat cells after stimulation. Data are the mean ± SEM from 2 independent experiments (n=24 cells). Statistical significance was determined by one-way ANOVA, with significance values indicated in figure. **e-f** hCD27$^+$ Jurkat NF-κB GFP reporter cells were stimulated with the indicated concentrations of either bivalent anti-hCD27 hIgG1 V11 (left panel) or Tetra anti-hCD27 hIgG1 V11 (right panel) in the presence of WT CHO cells (WT CHO), WT CHO cells and a goat anti-hFc f(ab)$_2$ (WT CHO + Xlink) or hFcγRIIB$^+$ CHO cells (hFcγRIIB$^+$ CHO). GFP reporter production was determined by flow cytometry and presented as **e** mean fluorescence intensity (MFI) of GFP$^+$ cells and **f** percentage of GFP$^+$ cells. Data points are the mean ± SEM (n=3) from 3 independent experiments. Statistical significance between hFcγRIIB$^+$ CHO and WT CHO + Xlink was determined by one-way ANOVA on AUC values, with significance values indicated in figure. Source data are provided as a Source Data file.

Editorial Summary

CD27 is a key T-cell costimulatory receptor, but efforts to target CD27 have been limited by the poor clinical efficacy of first-generation anti-CD27 antibodies. The authors here engineer higher-valency antibodies by more effectively engaging CD27 and selectively binding to FcγRIIB, which enhance anti-tumor activity.

Peer review information: *Nature Communications* thanks the anonymous reviewer(s) for their contribution to the peer review of this work. A peer review file is available.

A

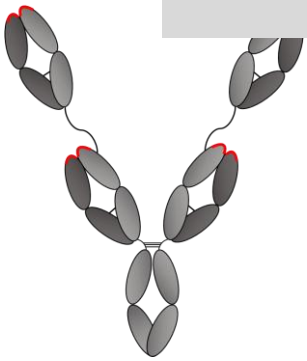

B

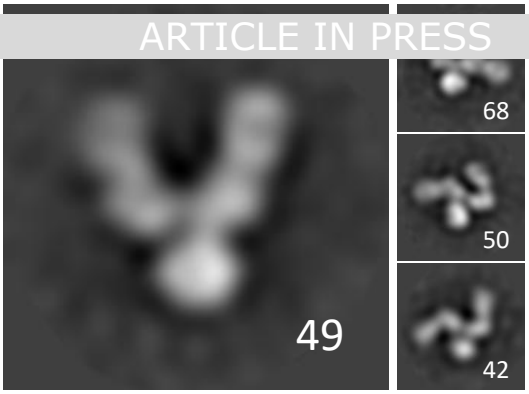

C

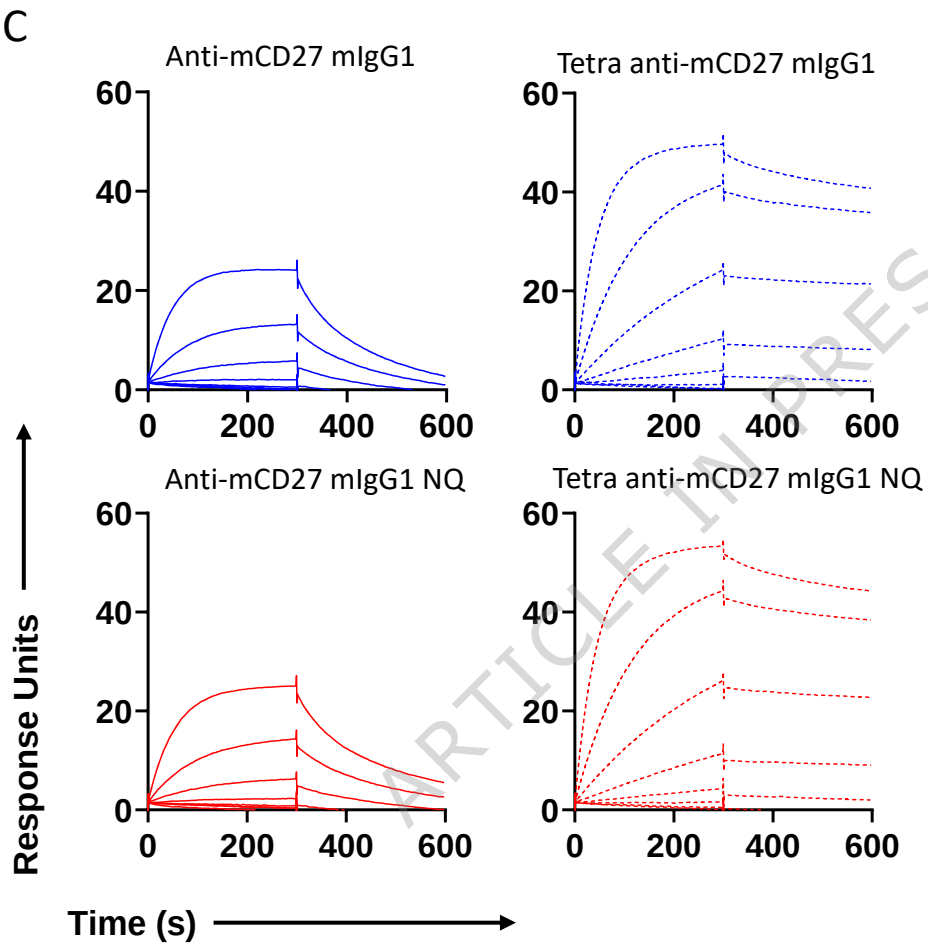

D

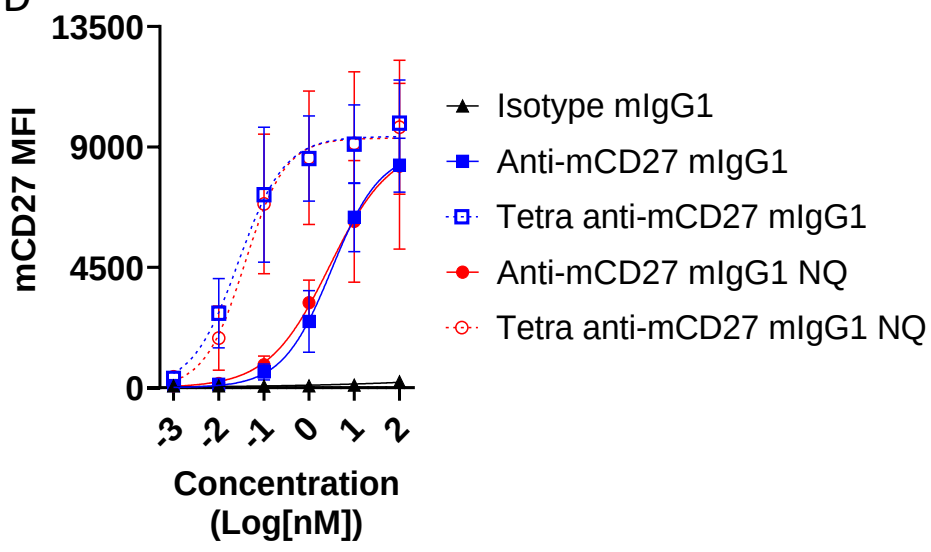

A

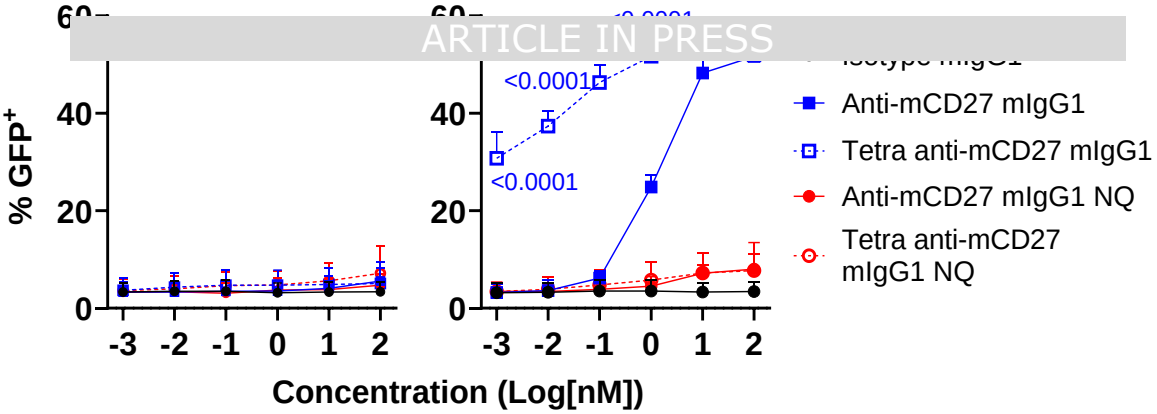

B

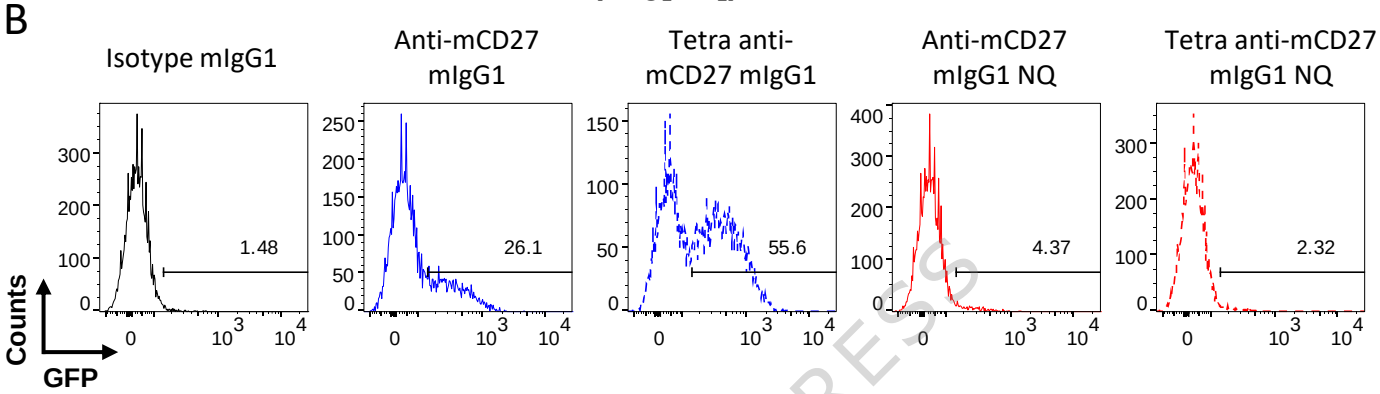

C